Nonlinear Dyn
DOI 10.1007/s11071-015-2485-3

REVIEW

Review and comparison of dry friction force models

Ettore Pennestrì · Valerio Rossi · Pietro Salvini · Pier Paolo Valentini

Received: 21 July 2015 / Accepted: 28 October 2015

Abstract Friction force models play a fundamental role for simulation of mechanical systems. Their choice affects the matching of numerical results with physically observed behavior. Friction is a complex phenomenon depending on many physical parameters and working conditions, and none of the available models can claim general validity. This paper focuses the attention on well-known friction models and offers a review and comparison based on numerical efficiency. However, it should be acknowledged that each model has its own distinctive pros and cons. Suitability of the model depends on physical and operating conditions. Features such as the capability to replicate stiction, Stribeck effect, and pre-sliding displacement are taken into account when selecting a friction formulation. For mechanical systems, the computational efficiency of the algorithm is a critical issue when a fast and responsive dynamic computation is required. This paper reports and compares eight widespread engineering friction force models. These are divided into two main categories: those based on the Coulomb approach and those established on the bristle analogy. The numerical performances and differences of each model have been monitored and compared. Three test cases are discussed: the Rabinowicz test and other two test problems casted for this occurrence.

Keywords Friction · Stiction · Stick–slip · Rabinowicz test · Pre-sliding · Bristle

E. Pennestrì (✉) · V. Rossi · P. Salvini · P. P. Valentini
Department of Enterprise Engineering, University of Rome Tor Vergata, Via del Politecnico 1, Rome, Italy
e-mail: pennestri@mec.uniroma2.it

V. Rossi
e-mail: valerio.rossi@uniroma2.it

P. Salvini
e-mail: salvini@uniroma2.it

P. P. Valentini
e-mail: valentini@ing.uniroma2.it

1 Introduction

Friction is a complex phenomenon with a key role in the study of mechanical systems. Early scientific studies refer to Leonardo da Vinci (1452–1519), Amontons (1663–1705), and Coulomb (1736–1806). The mathematical modeling of the friction force for the purpose of dynamic system simulation is crucial for the accuracy and reliability of the results.

Due to the abundance of excellent bibliographic sources (e.g., [1,38,45]), this paper does not dwell on the reasoning and algebraic treatment that brought to the deduction of friction models considered. This paper, after reporting the main equations, focuses on the computational performances of tangent friction force formulations for simple numerical test setups.

The classic Coulomb friction model [17] is herein adopted as example in the discussion about the macroscopic effects of friction. This model appears elementary from a mathematical point of view and straightforward to be implemented into a dynamic simulation

Published online: 11 November 2015

environment. In particular, the friction force, tangent to the contacting surface, is analytically expressed as follows:

$$F \begin{cases} \leq \mu_s F_n & v = 0 \\ = -\mu_d F_n \operatorname{sgn}(v) & v \neq 0 \end{cases} \tag{1}$$

where v is the relative velocity between the two bodies in single contact, μ_s the static friction coefficient, μ_d the dynamic friction coefficient, and F_n is the normal force. The force plot of the discontinuous Coulomb force function versus velocity is depicted in Fig. 1.

In our treatment, the normal force F_n is omitted in notation, and only the dynamic friction force $F_d = \mu_d F_n$ and the static friction force $F_s = \mu_s F_n$ will be mentioned. In order to simplify the Coulomb model [55], it is possible to get rid of the static friction force F_s and the Eq. (1) becomes:

$$F = -F_d \frac{v}{|v|} \tag{2}$$

Friction force is always opposite to the relative velocity when the velocity is $v \neq 0$. This produces numerical issues in terms of computational burden. Due to the discontinuity of friction force at zero velocity, the classic Coulomb model causes stiff equations of motion. In fact, during numerical integration the exact value $v = 0$ is never exactly matched. Variable step integration routines will reduce time step to account for sudden oscillating velocity values from positive, when $F = F_d$, to negative, when $F = -F_d$.

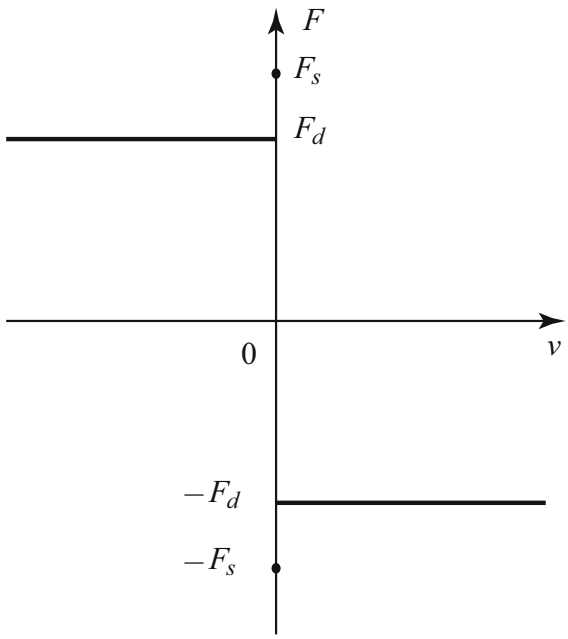

Fig. 1 The Coulomb friction force model

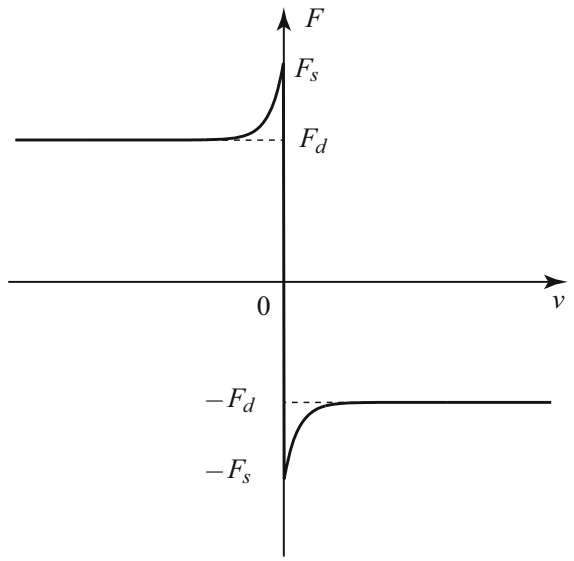

Fig. 2 Benson exponential friction model

The classic Coulomb model is not always accurate. Since mechanical contacts with distributed mass and compliance cannot exhibit an instantaneous change in force, the discontinuous friction model is a nonphysical simplification [6].

Although not observed by Coulomb, experimental evidence demonstrates a variation of friction force with the relative velocity v. In particular, three main regions can be identified in a plot of friction force versus v. The first region, with low v values, is well approximated by the Coulomb model. After a certain velocity limit and within a finite interval, a decrement of force is recorded. Outside such interval there is a slight increase in the friction force with speed. This dependency has been studied by many investigators [40]. However, the experimental friction force plots developed by Stribeck allowed to classify the tribology properties of surfaces and justify the association of his name with this phenomenon.

Many alternatives have been proposed to include the Stribeck effect and mitigate the problems linked to the classic Coulomb model for relative velocity values close to zero. For instance, the Benson friction model [8], depicted in Fig. 2, is available in the commercial software COMSOL Multiphysics® Structural Mechanics Module [16]. Benson friction force model is expressed with the following equation:

$$F = -F_d - (F_s - F_d)\mathrm{e}^{-c|v|}\,\mathrm{sgn}(v) \tag{3}$$

where c is the exponential decay constant.

A distinctive feature of friction models is the capability to account for stiction. During the stiction phase, there is not relative motion between the bodies at the point of contact ($v = 0$) [12]. Thoughtful reviews on friction models (e.g., [5,9,25]), including those with bristle effects [29], are available in technical literature. However, none of them reports on direct comparison of numerical efficiency performances and amount of dissipated energy. The monitoring of this physical variable is significant because friction models are often introduced to foresee energy losses under different operating conditions [37].

There is abundance of contributions regarding the improvement in the Coulomb friction model by making use of valuable mathematical algorithm. A reliable numerical tool proved to be the linear complementarity problem (LCP) [4,26,34,48,57], where a set of differential equations and inequalities are simultaneously solved. Nevertheless, LCP, currently not widespread in multibody dynamics commercial simulation codes, requires the availability of the full set of equations of motion for the entire mechanical system. This condition is critical for recursive dynamic formulations. Other researchers [61] add a constraint equation to deal with friction force and stiction (commercial code LMS Virtual.Lab Motion [36]).

In high-precision pointing and tracking operations, where small displacements and velocities are simulated, an accurate motion analysis during the stiction phase is a requirement. The macroscopic definition of stiction is a regime of several microns of motion where the friction force is mainly a function of displacement [5]. During this state, called pre-sliding displacement, some motion is possible even when a mechanism is stuck under the static friction force. However, the pre-sliding behavior is reproduced by some of the friction force models herein investigated.

The paper is organized in three main parts. In Sect. 2 the following friction models are discussed: the smooth Coulomb model, the velocity-based model (commercial code MSC Adams friction model), the Karnopp model, different variants of bristle models, such as the Dahl, LuGre, stick–slip model (embodied in the commercial code FunctionBay Recurdyn $^{\mathrm{TM}}$), elasto-plastic, and finally the Gonthier model. Section 3 describes the test cases adopted: the Rabinowicz test case, a test case with three bodies and multiple contacts and a test for proving pre-sliding model capabilities. Each of them can highlight the pros and cons of the tested friction models. Finally, in Sect. 4 the results are discussed and some elements for the choice of the friction model provided.

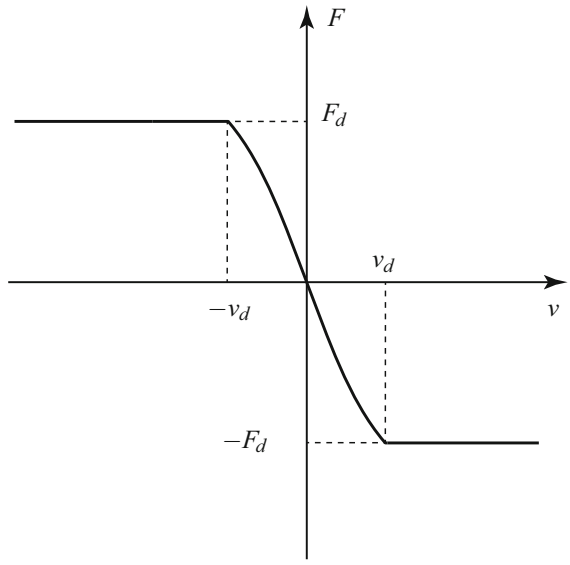

Fig. 3 Smooth Coulomb friction model

2 Friction models

In this section an analytic description of friction models is reported.

2.1 Smooth Coulomb model

The smooth Coulomb friction model, known also as continuous model [32], is a variation of the classic Coulomb model. It has been introduced to avoid the computational burden caused by the force discontinuity. As shown in Fig. 3, a smooth curve replaces the discontinuity around $v = 0$. Several smoothening functions [33] can be adopted to achieve the sought effect: linear [50], exponential [59] or trigonometric [20]. In this paper only the hyperbolic tangent smoothening function [42] will be investigated. Hence, the smooth Coulomb model can be formulated as

$$F = -F_d \tan h(v/v_d) \tag{4}$$

where v_d is the velocity tolerance. Since at zero velocity the force is null, this model cannot reproduce stiction. The main advantage is the gain in computational

stability which depends now on the chosen value of v_d. This is the friction model available in commercial codes such as DCAP [46] and SimPack [56].

2.2 Velocity-based model

The velocity-based friction model shares a similarity of approach with the previous one. There is only a different variation of the friction force with respect to the velocity. Within the interval including the zero velocity, an additional curve is introduced in an effort to mimic stiction. Figure 4 depicts the plot of the friction force versus velocity, where F_d denotes the dynamic friction force, F_s the static friction force, v_d the dynamic velocity tolerance and v_s the static velocity tolerance. The curve is a piecewise assembly of trigonometric functions with F_d, F_s, v_d and v_s as parameters. However, this model is far from reproducing stiction at zero velocity. Nevertheless, thanks to the friction force F_s, the relative velocity is reduced mainly with respect to the smooth Coulomb friction model. This friction model is available in the commercial code MSC Adams [43].

Some authors (e.g., [60]) hinted the use of the single expression:

$$F = -F_s \sin\Big[C \tan^{-1}(B \cdot v) - E\left\{(B \cdot v) - \tan^{-1}(B \cdot v)\right\}\Big] \tag{5}$$

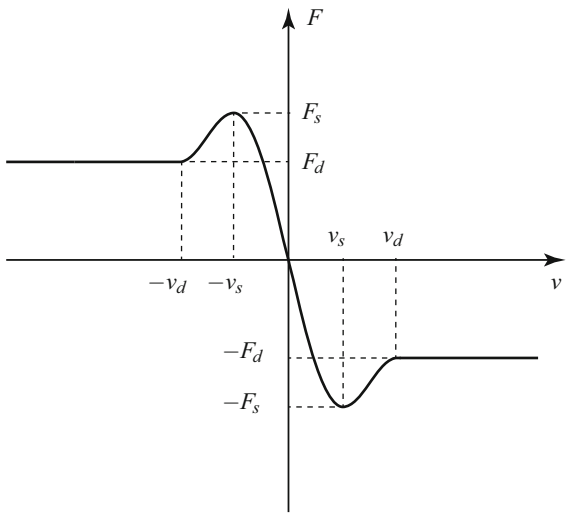

Fig. 4 Velocity-based friction model

where the shape of the function can be adjusted varying the parameters C, B, and E in order to match experiments.

2.3 Karnopp model

The Karnopp friction model [30] is pictorially represented in Fig. 5. This model somewhat can manage the stiction phenomenon [53]. Within the dead band $|v| < v_d$ stiction is assumed and the velocity is considered null. There are different ways to analytically express the Karnopp model [5]. In this paper we will adopt the one due to Borello and Dalla Vedova [11]:

$$F = \begin{cases} -\min\Big(\max(-F_s, F_{\text{ext}}), F_s\Big) & |v| \le v_d \\ -F_d \operatorname{sgn}(v) & |v| > v_d \end{cases} \tag{6}$$

where F_{ext} is the resultant of the active external forces. Within the tolerance region, the friction force is always less or equal, and opposite, to the resultant of the active external forces. This friction model can simulate stiction and is very convenient from a computational point of view. The main drawback is the need to know the resultant of the external forces F_{ext}. In a mechanical system with more than one contact per body, the evaluation of F_{ext} is not an easy task. A distinction between several cases is needed, as explained by Karnopp [30]. The identification of the model parameters is also of interest [54].

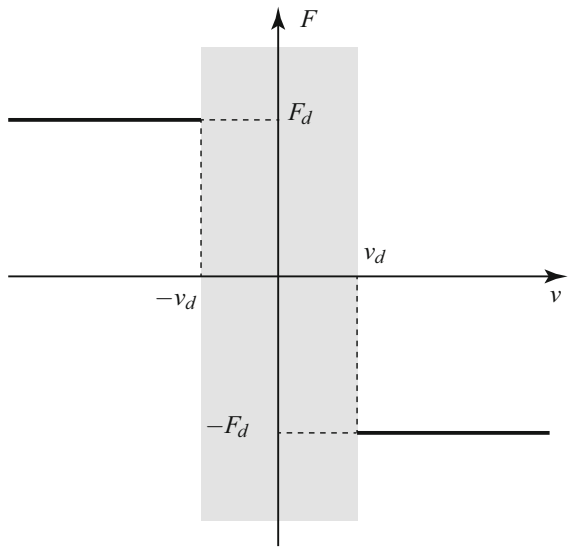

Fig. 5 Karnopp friction model

2.4 Dahl model

The Dahl friction model [15,18] is basically a Coulomb friction model with a lag in the change of the friction force during the switching of the direction of motion.

The Dahl model is commonly described as a bristle model, as shown in Fig. 6. Within a given applied load, the elastically deformed bristle adds a compliance and returns to its original position after the load is removed. Once the elastic resistance is overtaken, the entire brush moves and a permanent displacement is produced. By means of this dynamics, the Dahl model includes a lag when the velocity v changes sign. The Dahl friction force bears similarities with a spring force and can be expressed as follows

$$F = -\sigma_0 z \tag{7}$$

where σ_0 is the stiffness of the bristle and z the internal variable representing the relative displacement. The state variable z is obtained from

$$\dot{z} = v \cdot \left(1 - \frac{\sigma_0 z}{F_d}\,\mathrm{sgn}(v)\right)^{\alpha}, \tag{8}$$

where α is a parameter influencing the shape of the friction force variation within the interval $1 < \alpha < 2$.

The Dahl model is substantially different from the Coulomb approach. It requires an additional state which needs to be numerically integrated during the simulation. The stiction effect, corresponding to elastic range of the bristle movement, can be reproduced. Since there is not relation between friction force F_d and relative velocity, the Stribeck effect cannot be reproduced.

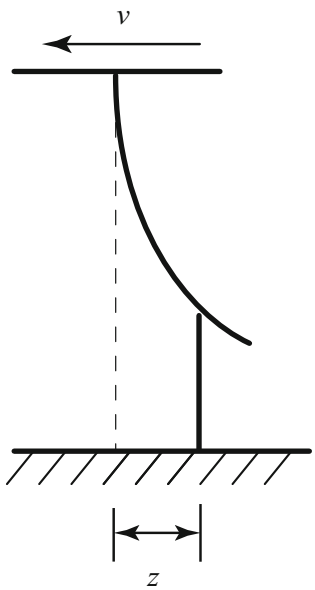

Fig. 6 The bristle analogy in the Dahl model

From the Dahl model numerous models have been developed to improve the reliability of the results [28]. The Bliman–Sorine friction model [10] can be interpreted as a parallel connection of two Dahl models. The use of Dahl model in planar multibody systems is documented in [47]. Several contributions [2,19,31] focus on the parameters calibration and identification.

2.5 LuGre model

The LuGre friction model [7,49] develops the one of Dahl with some significant improvements. The model name is an acronym obtained from the initials of the cities (Lund and Grenoble) of the research groups that proposed the model [13]. The friction force equation is hereinafter reported

$$F = \sigma_0 z + \sigma_1 \dot{z} + \sigma_2 v \tag{9}$$

where σ_0 is a stiffness, like in the Dahl model, σ_1 is a micro damping and σ_2 is the viscous damping. The state variable z is expressed as

$$\dot{z} = v \cdot \left(1 - \frac{\sigma_0 z}{g(v)}\,\mathrm{sgn}(v)\right) \tag{10}$$

where $g(v)$ is a velocity-dependent function which can reproduce both Coulomb friction and Stribeck effect. Considering a typical approximation of the Stribeck effect, it is convenient to express $g(v)$ as

$$g(v) = F_d + (F_s - F_d)\mathrm{e}^{-(v/v_{\mathrm{Stribeck}})^{\gamma}} \tag{11}$$

where each parameter has been already introduced in the previous subsection and v_{Stribeck} is the Stribeck velocity, i.e., the velocity at which the steady-state friction force starts decreasing). A value of $\gamma = 2$ is in good agreement in most of the cases [44].

To simplify the model, the relative motion between the sliding surfaces can be considered to be quasi-static [35] and the velocity $\dot{z} \to 0$. The quasi-static form of the LuGre friction model is

$$F = \left(F_d + (F_s - F_d)\mathrm{e}^{-(v/v_s)^{\gamma}}\right)\mathrm{sgn}(v) + \sigma_2 v \tag{12}$$

2.6 Elasto-plastic model

The elasto-plastic friction model [21,22] is considered an enhancement of the LuGre model.

Stiction can be described as the condition where the micro displacement z is less than a breakaway displacement $|z| < z_{ba}$. In this case the only possible motion of the surface consists entirely of elastic displacement, which is called pre-sliding displacement. This is analogous to the elastic deformation observed in a stress–strain curve. The breakaway displacement can be associated with the strain at which plastic deformation begins. The friction force follows from the one of the LuGre model

$$F = \sigma_0 z + \sigma_1 \dot{z} + \sigma_2 v \tag{13}$$

but the derivative of the state variable is

$$\dot{z} = v \cdot \left(1 - \alpha(z, v)\frac{\sigma z}{g(v)}\,\mathrm{sgn}(v)\right) \tag{14}$$

where $\alpha(z, v)$ is an additional parameter used to include pre-sliding displacement and stiction. If $\mathrm{sgn}(v) = \mathrm{sgn}(\dot{z})$, then the $\alpha(z, v)$ parameter takes the following values, as shown in Fig. 7:

$$\alpha(z, v) = \begin{cases} 0 & |z| < z_{ba} \\ \frac{1}{2}\left(1 + \sin\left(\pi \frac{z - \frac{1}{2}(z_{\max} + z_{ba})}{z_{\max} - z_{ba}}\right)\right) & z_{ba} \le |z| < z_{\max} \\ 1 & |z| \ge z_{\max} \end{cases} \tag{15}$$

where $z_{\max} = \frac{g(v)}{\sigma_0}$. Otherwise, if $\mathrm{sgn}(v) \neq \mathrm{sgn}(\dot{z})$ then $\alpha(z, v)$ is set equal to zero.

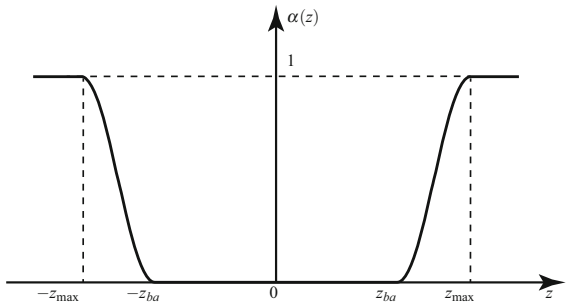

Fig. 7 Elasto-plastic friction model $\alpha(z)$ parameter in case of $\mathrm{sgn}(v) = \mathrm{sgn}(\dot{z})$

Table 1 Stick–slip parameters in case of either stiction and sliding conditions

State	Sliding	Stiction
v	$\lvert v\rvert > v_t$	$0 \le \lvert v\rvert \le v_t$
β	1	$\mathrm{Step}(\lvert v\rvert, -v_t, -1, v_t, 1)$
F_s	0	$\mathrm{Step}(\lvert F_s\rvert, -\Delta_{\max}, -F_s, \Delta_{\max}, F_s)$
F_d	F_d	$\mathrm{Step}(\lvert F_d\rvert, -v_t, -F_d, v_t, F_d)$
F	F_{sliding}	$F_{\mathrm{stiction}} + F_{\mathrm{sliding}}$

2.7 Stick–slip model

The stick–slip friction model [14] is again based on the assumption of a spring type force under stiction conditions. As observed for the Dahl and LuGre models, also the stick–slip friction model introduces a state variable, namely a deformation, for the computation of the friction force during the stiction phase. Hence, the friction force is divided in two contributions

$$F = F_{\mathrm{stiction}} + F_{\mathrm{sliding}} \tag{16}$$

where F_{stiction} and F_{sliding} represent the friction force during stiction and sliding phase, respectively. Those forces are expressed as follows:

$$F_{\mathrm{stiction}} = -(1 - \beta) F_s\,\mathrm{sgn}(\Delta) \tag{17}$$

$$F_{\mathrm{sliding}} = -F_d\,\mathrm{sgn}(v) \tag{18}$$

where Δ corresponds to the Dahl z parameter of Fig. 6 and β is a parameter which depends on the velocity. Like the Coulomb friction force F_d, the F_{sliding} appears away from the stiction phase. F_{stiction} depends on several parameters, as specified in Table 1 where v_t is a threshold velocity and $\Delta_{\max}$ the maximum stiction deformation. The step function mentioned in Table 1 regulates the transition from stiction to dynamic conditions is expressed as follows

$$\mathrm{step}(x, x_0, h_0, x_1, h_1) = \begin{cases} h_0 & x \le x_0 \\ h_0 + (h_1 - h_0)\left(\frac{x - x_0}{x_1 - x_0}\right)^2 & \\ \quad \left(3 - 2\left(\frac{x - x_0}{x_1 - x_0}\right)\right) & x_0 < |x| < x_1 \\ h_1 & x \ge x_1 \end{cases} \tag{19}$$

Figure 8 shows the shape of the step function for generic parameter values.

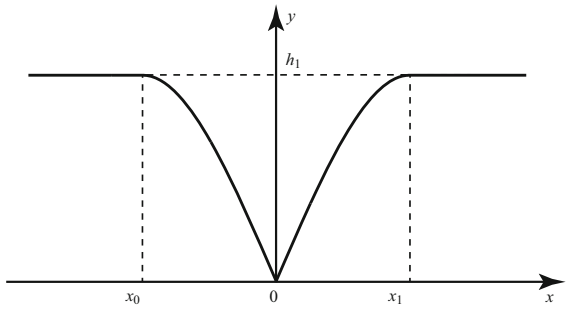

Fig. 8 Behavior of the step function $y = \text{step}(|x|, x_0, h_0, x_1, h_1)$

The stick–slip friction model is implemented in the multibody commercial software FunctionBay Recurdyn^{TM} [23].

2.8 Gonthier model

In the Gonthier friction model [27], the relationship between static friction and the time of contact is a variant of the LuGre model. The Gonthier model relies again upon the bristle approach. A physical time lag effect, called dwell time, is introduced. The friction force is estimated by means of the formula

$$F_{br} = \sigma_0 z + \sigma_1 \dot{z} \tag{20}$$

where the σ_0 and σ_1 have the same meaning of the LuGre model parameters, as reported in Sect. 2.5. The state variable z is composed of two contributions

$$\dot{z} = s\dot{z}_{st} + (1 - s)\dot{z}_{sl} \tag{21}$$

where $\dot{z}_{st}$ and $\dot{z}_{sl}$ refer to the sticking and sliding condition, respectively. The variable s, which allows a smooth transition between the friction regimes, is computed by means of the formula

$$s = \mathrm{e}^{-v^2/v_{\text{Stribeck}}^2} \tag{22}$$

where v_{Stribeck} is the Stribeck velocity. The sticking and sliding terms are defined as follows

$$\dot{z}_{st} = v \tag{23}$$

$$\dot{z}_{sl} = \frac{1}{\sigma_1} F_c - \frac{\sigma_0}{\sigma_1} z \tag{24}$$

where F_c is

$$F_c = F_d \cdot \text{dir}(v, v_t) \tag{25}$$

and the function $\text{dir}(v, v_t)$

$$\text{dir}(v, v_t) = \begin{cases} \dfrac{v}{|v|} & |v| \geq v_t \\ \dfrac{v}{v_t}\left[\dfrac{3}{2}\dfrac{|v|}{v_t} - \dfrac{1}{2}\left(\dfrac{|v|}{v_t}\right)^3\right] & |v| < v_t \end{cases} \tag{26}$$

The expression of the maximum stiction force is

$$F_{\max} = F_d + (F_s - F_d)s_{dw} \tag{27}$$

where s_{dw} is the internal state variable introduced to model the dwell-time effect. This variable follows from numerical integration of

$$\dot{s}_{dw} = \begin{cases} \dfrac{1}{\tau_{dw}}(s - s_{dw}) & (s - s_{dw}) \geq 0 \\ \dfrac{1}{\tau_{br}}(s - s_{dw}) & (s - s_{dw}) < 0 \end{cases} \tag{28}$$

where τ_{dw} is the dwell-time dynamics time constant and τ_{br} is the bristle dynamics time constant defined as $\tau_{br} = \sigma_1/\sigma_0$. Therefore, the total friction force is

$$F = -\text{sat}(F_{br}, F_{\max}) - \sigma_2 v \tag{29}$$

where $\text{sat}(F_{br}, F_{\max})$ is a saturation function

$$\text{sat}(F_{br}, F_{\max}) = \begin{cases} F_{br} & |F_{br}| \leq F_{\max} \\ \dfrac{F_{br}}{|F_{br}|} F_{\max} & |F_{br}| > F_{\max} \end{cases} \tag{30}$$

The Gonthier friction model requires the definition of the following parameters: F_d, F_s, σ_0, σ_1, σ_2, τ_{dw}, v_{Stribeck}. The author recommends that the parameter v_t should be at least one-tenth of v_{Stribeck} [27].

3 Numerical simulations

Table 2 summarizes the parameters required by each of the friction models discussed.

A MATLAB code has been developed to compare the friction models previously discussed. Three test cases have been considered to gather direct experience and compare the performances of each model under different operating conditions.

Three numerical integration routines of the standard MATLAB ODE Solvers library have been tested in conjunction with the friction models discussed:

- `ode45`: explicit variable step Runge–Kutta fourth- and fifth-order method;
- `ode113`: multistep solver with a variable order Adams–Bashforth–Moulton PECE algorithm;

Table 2 Summary of model parameters and state variables

Model	Parameters	State variable
Coulomb	F_d,v_d	
Velocity based	F_d, F_s, v_d, v_s	
Karnopp	F_d, F_s, v_d	
Stick–slip	F_d, F_s, v_t, $\Delta_{\max}$	
Dahl	F_d, σ_0, α	z
LuGre	F_d, F_s, σ_0, σ_1, σ_2, v_{Stribeck}, γ	z
Elasto-plastic	F_d, F_s, σ_0, σ_1, σ_2, v_{Stribeck}, γ, z_{ba}	z
Gonthier	F_d, F_s, σ_0, σ_1, σ_2, v_{Stribeck}, v_t, τ_{dw}	z, s_{dw}

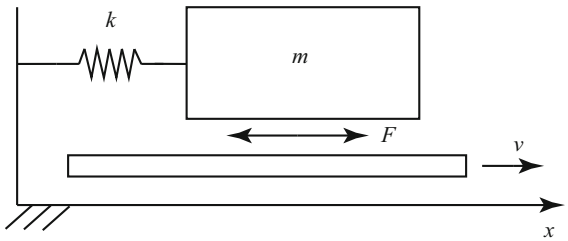

Fig. 9 Rabinowicz test case

– `ode15s`: multistep solver with a variable order solver based on the numerical differentiation formulas, suitable for stiff problems.

Different relative errors tolerances `RelTol` have been used. In particular, the followings have been set as integrator options: 10^{-4}, 10^{-6} and 10^{-8}.

It should be acknowledged that the friction parameters affect efficiency and accuracy of the models herein considered. With the purpose of a comparison on a similar basis, whenever possible, the same numerical parameters have been used.

3.1 Rabinowicz test case

The Rabinowicz test case [51] is one experiment aimed to study the stick–slip behavior in a mechanical system. Different contributions [3,24,39,41,58] agree to consider it as a benchmark for the evaluation of friction force models.

With reference to the scheme of Fig. 9, a spring of stiffness k connects a body of mass m to the inertial reference frame. A slab below the body is translating

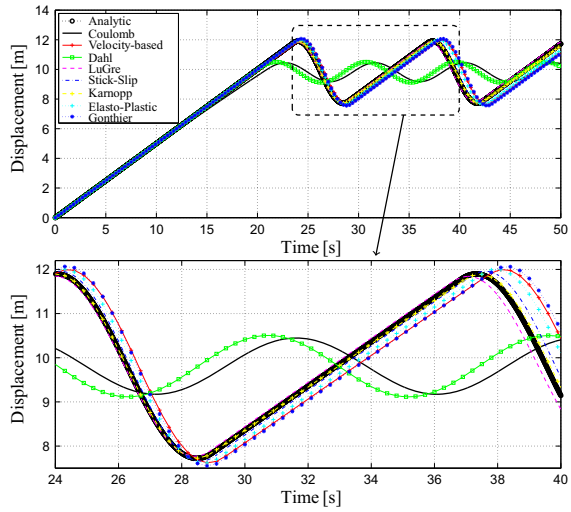

Fig. 10 Displacement of the body for the Rabinowicz test case

at a constant velocity v. A friction force F originates at interface between the slab and the body. Initially the body is dragged along the moving slab. The spring does not hold back the body until the spring pull equals the static friction force. At this point, the body begins to slip on the moving surface and the friction force (dynamic friction force) is lower than the one recorded at the previous state. After a while, the mass motion is halted. The static friction force takes over and the body sticks to the surface of the slab. The process repeats for the length of the simulation.

The assigned parameter values are: $m = 20\,\text{kg}$, $k = 10\,\text{N/m}$ and $v = 0.5\,\text{m/s}$. A Coulomb dynamic friction coefficient of $\mu_d = 0.5$ and a Coulomb static friction coefficient of $\mu_s = 0.6$ produce the following friction forces: $F_d = 98.1\,\text{N}$ and $F_s = 117.72\,\text{N}$. The parameters for the Dahl, LuGre, elasto-plastic, and Gonthier models, assumed proportional to the friction force, are $\sigma_0 = 98{,}100\,\text{N/m}$, $\sigma_1 = 780\,\text{Ns/m}$, $\sigma_2 = 0\,\text{Ns/m}$ and $\alpha = \gamma = 1$. The stick–slip model parameters are $v_t = 0.05\,\text{m/s}$ and $\Delta_{\max} = 10^{-4}\,\text{m}$, while $z_{ba} = 10^{-4}\,\text{m}$ is adopted for the simulation of the elasto-plastic model. The following velocity tolerances have been used: $v_d = v_{\text{Stribeck}} = 0.05\,\text{m/s}$ and $v_s = 0.01\,\text{m/s}$. The parameters $v_t = 5 \times 10^{-4}\,\text{m/s}$ and $\tau_{dw} = 0.1\,\text{s}$ have been adopted for the Gonthier model.

Figure 10 reports the plots of body displacement versus time. The first item in the legend represents the closed-form solution computed assuming an harmonic oscillator subjected to Coulomb friction (e.g.,

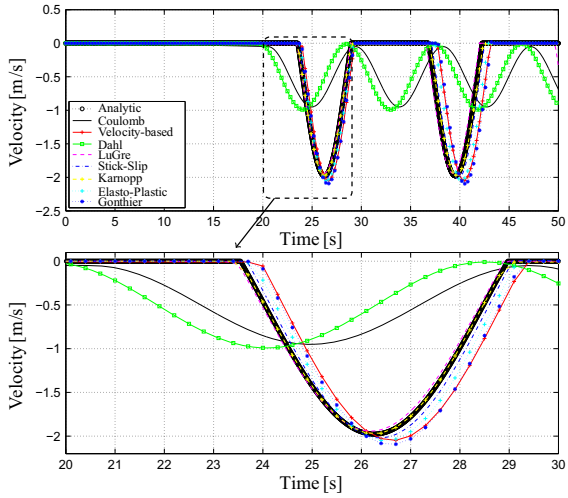

Fig. 11 Relative velocity of the body with respect to the slab for the Rabinowicz test case

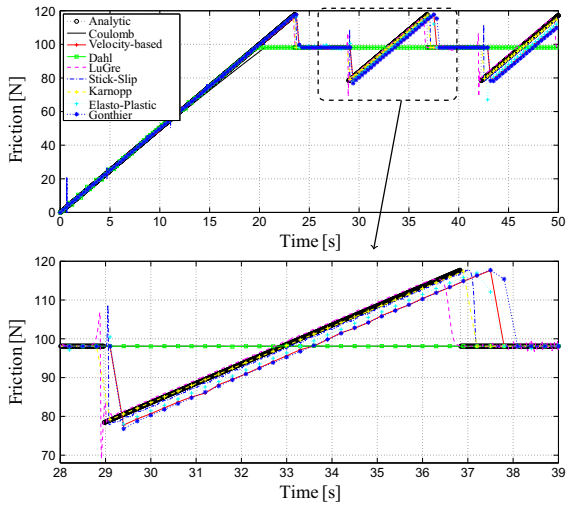

Fig. 12 Friction force for the Rabinowicz test case

[52]). Although the analytic solution is consistent from a mathematical point of view with the classic Coulomb model, not necessarily represents the most appropriate simulation of the physical phenomenon. Since they cannot account for any static friction force, the smooth Coulomb model and the Dahl model have a distinct behavior. The plot of the relative velocity between the body and the slab versus time is depicted in Fig. 11. The stiction phase can be identified observing the flat zones of the plot.

Finally, the friction force magnitude and system kinetic and potential energy plots, for each friction model, are respectively summarized in Figs. 12 and 13.

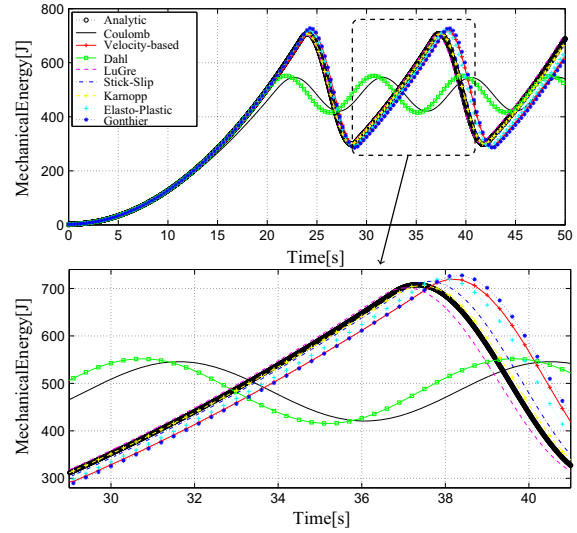

Fig. 13 System kinetic and potential energy for the Rabinowicz test case

The LuGre model shows sharp oscillations that could be smoothed by means of parameters tuning. For this test case, and with the exception of smooth Coulomb and Dahl models, the system energy plots for the models under test are almost overlapped. This demonstrates a substantial equivalence of the amount of dissipated energy.

Computing time has been measured with tools available in the MATLAB environment. This time may change due to simultaneous background tasks of the operating system. For this reason, average values have been herein reported. Table 3 compares the normalized Ψ_i computing time needed by each friction model. The following relation is adopted

$$\Psi_i = \frac{T_i}{T_{\max}} \cdot 100 \tag{31}$$

T_i is the computing time needed to simulated the observed friction model and $T_{\max}$ the maximum of the T_i's.

Tables 4 and 5 summarize the numerical differences between each friction model and the analytic solution. These differences ξ_i and Γ_i are computed as follows:

$$\xi_i = \max \left| \frac{x_i - x_{\text{an}}}{x_i} \right| \cdot 10^2$$
$$\Gamma_i = \frac{1}{n} \sum_{j=1}^{n} \left| \frac{x_{i_j} - x_{\text{an}_j}}{x_{i_j}} \right| \cdot 10^2 \tag{32}$$

where

Table 3 Normalized computing time Ψ [%] for the Rabinowicz test case

Model	Solver								
	`ode45`			`ode113`			`ode15s`		
	10^{-4}	10^{-6}	10^{-8}	10^{-4}	10^{-6}	10^{-8}	10^{-4}	10^{-6}	10^{-8}
Coulomb	7	4	4	7	6	6	7	3	3
Velocity based	100	86	88	77	81	77	4	5	5
Dahl	26	26	26	29	30	30	3	19	20
LuGre	25	24	25	28	28	28	4	6	7
Stick–slip	26	27	27	26	28	28	2	4	4
Karnopp	2	2	2	2	2	2	2	3	3
Elasto-plastic	31	28	29	31	31	31	4	6	6
Gonthier	10	11	11	10	11	11	10	11	11

Table 4 Maximum relative difference ξ [%] of each friction model compared to the analytic solution for the Rabinowicz test case

Model	Solver								
	`ode45`			`ode113`			`ode15s`		
	10^{-4}	10^{-6}	10^{-8}	10^{-4}	10^{-6}	10^{-8}	10^{-4}	10^{-6}	10^{-8}
Coulomb	27.3	27.3	27.3	27.3	27.3	27.3	27.3	27.3	27.3
Velocity based	12.5	12.5	12.5	12.5	12.5	12.5	12.4	12.5	12.5
Dahl	23.6	23.6	23.6	23.6	23.6	23.6	23.6	23.6	23.6
LuGre	3.8	4.0	4.0	3.8	4.0	4.0	4.6	4.0	4.0
Stick–slip	4.4	3.9	4.0	4.3	4.0	4.2	1824	3.9	4.0
Karnopp	1.9	2.1	2.1	2.1	2.1	2.1	2.0	2.1	2.1
Elasto-plastic	9.4	9.5	9.5	9.4	9.5	9.5	9.0	9.5	9.5
Gonthier	14.0	14.0	14.0	14.0	14.0	14.0	14.0	14.0	14.0

Table 5 Average relative difference Γ [%] of each friction model compared to the analytic solution for the Rabinowicz test case

Model	Solver								
	`ode45`			`ode113`			`ode15s`		
	10^{-4}	10^{-6}	10^{-8}	10^{-4}	10^{-6}	10^{-8}	10^{-4}	10^{-6}	10^{-8}
Coulomb	7.9	7.9	7.9	7.9	7.9	7.9	7.9	7.9	7.9
Velocity based	2.7	2.7	2.7	2.7	2.7	2.7	2.6	2.7	2.7
Dahl	6.9	6.9	6.9	6.9	6.9	6.9	6.9	6.9	6.9
LuGre	0.7	0.8	0.8	0.7	0.8	0.8	0.9	0.8	0.8
Stick–slip	0.8	0.8	0.8	0.8	0.8	0.8	99.0	0.8	0.8
Karnopp	0.3	0.3	0.3	0.3	0.3	0.3	0.3	0.3	0.3
Elasto-plastic	1.8	1.9	1.9	1.8	1.9	1.9	1.8	1.8	1.8
Gonthier	2.8	2.8	2.8	2.8	2.8	2.8	2.8	2.8	2.8

- x_i is the generic displacement value for the given friction model;
- x_{an} is the displacement for the analytic solution of the Coulomb model;
- j is the array index and n the computed displacement array length.

It should be observed that Tables 4 and 5 summarize the quantitative differences between models in terms

of maximum mass displacement. The term "error" has been avoided in favor of the term "difference." For the comparison, the analytic solution of the Coulomb model has been arbitrarily chosen as reference and not because it is the most accurate representation of the actual friction.

Regarding computing efficiency, from Table 3 one can observe that:

- the velocity-based, Dahl, LuGre, stick–slip, and elasto-plastic models should be used with a stiff solver such as `ode15s`;
- with the stiff solver, the Dahl model seems affected also by the value of the `RelTol` parameter;
- Karnopp and Gonthier models are not apparently influenced by the solver.

From Tables 4 and 5 one can infer that most of the models are not affected by the choice of the ODE solver and `RelTol` parameter. However, according to our experience, it is not recommended the use of the stick–slip model in conjunction with a stiff solver and a low `RelTol` parameter.

3.2 3-DOF test case

Figure 14 shows the topology of the proposed test case, herein named 3-DOF. Three bodies are stacked one on top of the other. Dry friction force is assumed in the contacts between the bodies. This test is useful to ascertain how a friction model handles the case of multiple friction forces acting on the same body.

Initially, the body 1 has an offset of 1 m with respect to the rest position. The spring has a stiffness of $k = 30\,\mathrm{N/m}$ and all the bodies have the same mass $m_1 = m_2 = m_3 = 2\,\mathrm{kg}$. The parameter values are reported in array notation for the three bodies in the system. The friction forces are

$$F_d = \left[\,9.81\ 3.92\ 11.77\,\right]^{\mathrm{T}}\ \mathrm{N}$$

$$F_s = \left[\,14.71\ 5.88\ 17.66\,\right]^{\mathrm{T}}\ \mathrm{N}$$

The parameters for the Dahl, LuGre, elasto-plastic, and Gonthier models, assumed proportional to the friction forces, are

$$\sigma_0 = \left[\,98100\ 39200\ 117700\,\right]^{\mathrm{T}}\ \mathrm{N/m}$$

$$\sigma_1 = \left[\,49\ 20\ 59\,\right]^{\mathrm{T}}\ \mathrm{Ns/m}$$

and $\sigma_2 = 0\,\mathrm{Ns/m}$, $\alpha = \gamma = 1$ for all contacts. The stiffness parameters are assumed proportional to the dynamic friction force acting on each contact. Similarly, for all contacts, the stick–slip model parameters are $v_t = 0.1\,\mathrm{m/s}$ and $\Delta_{\max} = 10^{-4}\,\mathrm{m}$. The elasto-plastic model breakaway deformation is $z_{ba} = 10^{-4}\,\mathrm{m}$. The friction models set $v_d = v_{\mathrm{Stribeck}} = 0.1\,\mathrm{m/s}$ and $v_s = 10^{-2}\,\mathrm{m/s}$ as velocity thresholds. The parameters $v_t = 0.1\,\mathrm{m/s}$ and $\tau_{dw} = 0.1\,\mathrm{s}$ have been adopted for the Gonthier model.

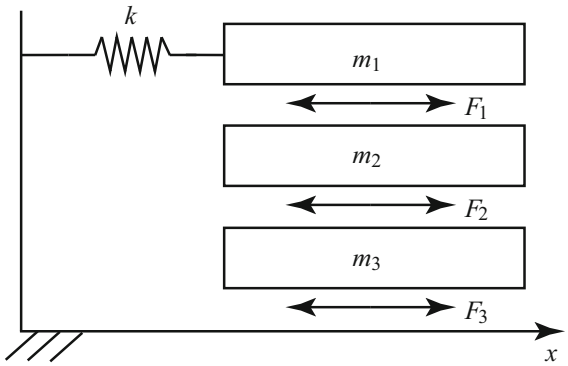

Fig. 14 3DOF test case

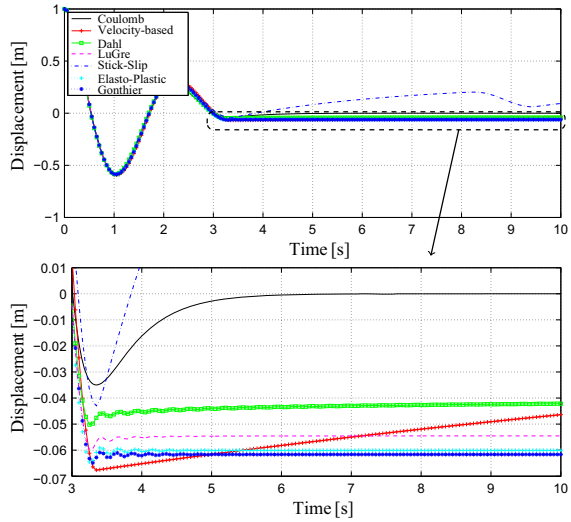

Fig. 15 Displacement of the first body for the 3-DOF test case

For this test case, the Karnopp friction model has not been investigated because the determination of the resultant of applied forces is demanding and not convenient for a case of multiple contacts on the same body.

Figure 15 shows the displacement of the first body. After the first oscillation, the stiction phase begins at the lower body. In a smooth Coulomb friction model,

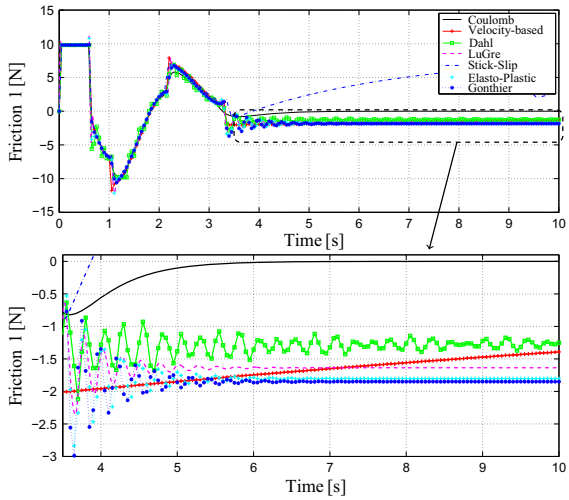

Fig. 16 Friction force F_1 for the 3-DOF test case

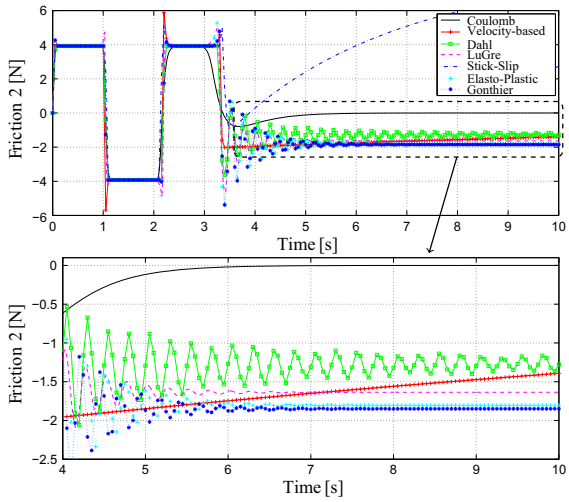

Fig. 17 Friction force F_2 for the 3-DOF test case

since there is no stiction force, the body slowly goes back to the rest position.

Figures 16, 17 and 18 report the friction forces F_1, F_2 and F_3. The critical phase of the simulation, for each friction model, is after the first 3 s when the bodies are stacked on top of each other. The Dahl friction model presents an oscillatory behavior with respect to the LuGre friction model due to lack of a damping term. The stick–slip friction model is indeed sensitive to the parameter values and after a certain amount of time a drift is observed. Figure 19 plots the system kinetic and potential energy versus time. Also for this test case, the

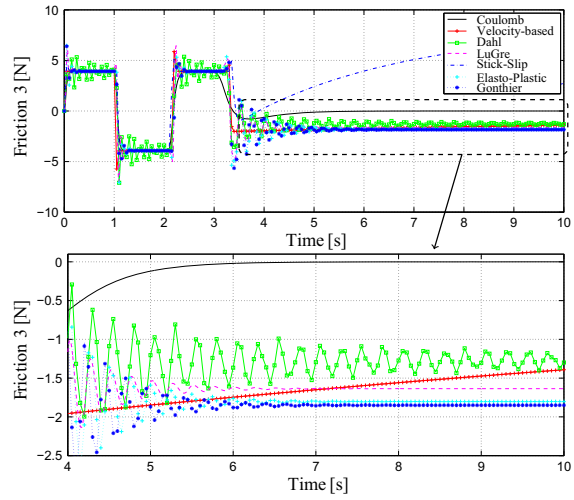

Fig. 18 Friction force F_3 for the 3-DOF test case

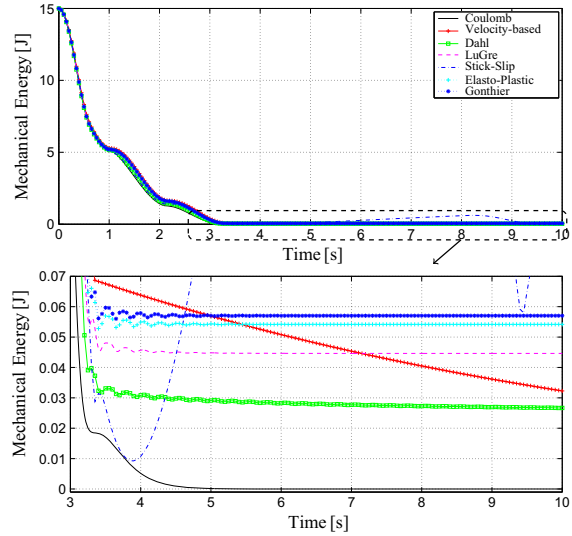

Fig. 19 System kinetic and potential energy for the 3DOF test case

energy plots, with the exception of the stick–slip model, can be almost overlapped.

Table 6 reports the normalized computing time Ψ. Regarding computing efficiency for this test case:

- the use of the velocity-based model with a stiff ODE solver is recommended;
- all the models, with the exception of the velocity-based model, are not apparently affected by the choice of the ODE solver and `RelTol` parameter.

Table 6 Normalized computing time Ψ [%] for the 3DOF test case

Model	Solver								
	`ode45`			`ode113`			`ode15s`		
	10^{-4}	10^{-6}	10^{-8}	10^{-4}	10^{-6}	10^{-8}	10^{-4}	10^{-6}	10^{-8}
Coulomb	3	1	1	2	2	1	3	1	1
Velocity based	99	97	100	77	78	75	5	4	4
Dahl	5	5	5	6	6	6	7	8	8
LuGre	4	4	4	4	4	4	3	4	4
Stick–slip	6	6	6	6	6	6	3	4	4
Elasto-plastic	5	5	5	5	5	5	3	4	4
Gonthier	3	4	4	3	4	4	3	4	4

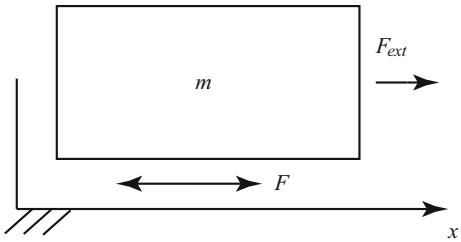

Fig. 20 Pre-sliding test case topology

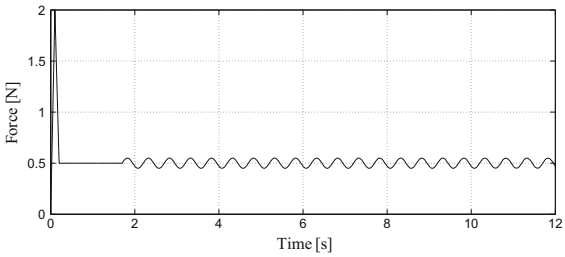

Fig. 21 Pre-sliding external applied force

3.3 Pre-sliding test case

To study the pre-sliding properties of each model, an interesting test has been proposed by Dupont et al. [22]. Figure 20 shows the simple single-degree-of-freedom system where a body is in contact with the ground and is excited by an external force.

The external force is a particular function which has an initial sudden peak of 2 N and then is harmonic with a mean value of 0.5 N and a frequency of 2 Hz, as shown in Fig. 21. The body has a mass of $m = 1\,\text{kg}$ and the dynamic and static friction forces are $F_d = 1\,\text{N}$ and $F_s = 1.1\,\text{N}$, respectively. After the first peak the external force has a magnitude smaller than the static friction force. Hence, the only movement allowed is the pre-sliding displacement.

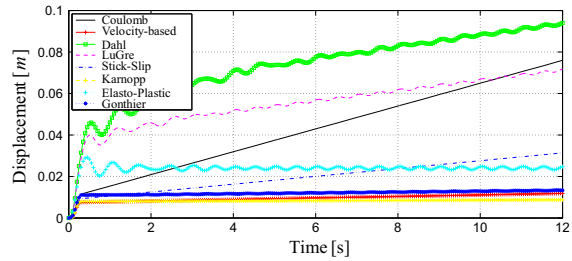

Fig. 22 Displacement plot of the body for the pre-sliding test case

The prescribed parameters for the Dahl, LuGre, elasto-plastic, and Gonthier models, assumed proportional to the friction force, are $\sigma_0 = 100\,\text{N/m}$, $\sigma_1 = 2\,\text{Ns/m}$, $\sigma_2 = 0\,\text{Ns/m}$ and $\alpha = \gamma = 1$. The stick–slip model parameters are $v_t = 0.01\,\text{m/s}$ and $\Delta_{\max} = 0.01\,\text{m}$ while $z_{ba} = 0.01\,\text{m}$ is adopted in the elasto-plastic model. The following velocity thresholds have been set: $v_d = v_{\text{Stribeck}} = 0.01\,\text{m/s}$ and $v_s = 10^{-4}\,\text{m/s}$. The parameters $v_t = 10^{-4}\,\text{m/s}$ and $\tau_{dw} = 0.01\,\text{s}$ have been adopted for the Gonthier model.

Figures 22 and 23 show the body displacement plots for all friction models herein discussed. A pronounced drift due to the lack of the stiction force is observed for the smooth Coulomb friction model. The velocity-based friction model exhibits a good behavior due to the small tolerance on the static velocity v_s. The Dahl and LuGre friction models have a tendency to drift even if they show a characteristic pre-sliding trend. The Karnopp model does not display any tendency to drift but is unable to simulate the pre-sliding displacement. The stick–slip friction model drifts like the smooth

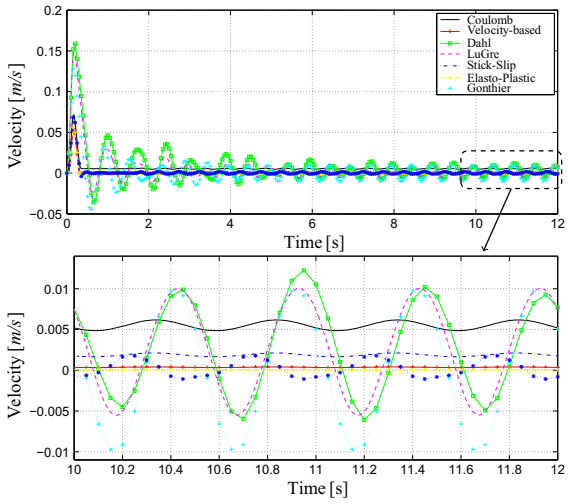

Fig. 23 Velocity plot of the body for the pre-sliding test case

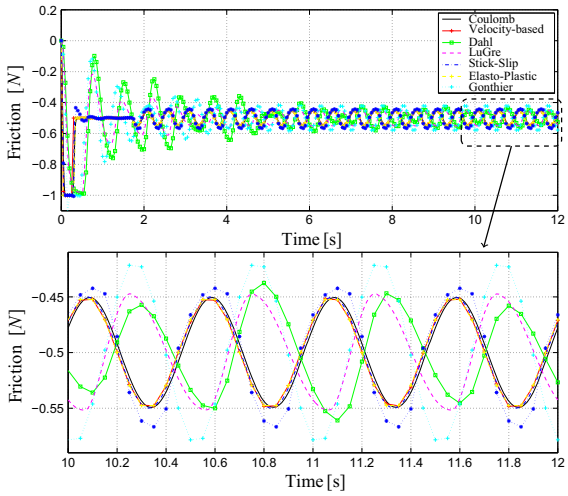

Fig. 24 Friction force plot for the pre-sliding test case

Coulomb model. Finally, for this kind of simulation, good performances of the elasto-plastic and Gonthier friction models are observed. Figures 24 and 25 report respectively the friction force and the system kinetic and potential energy. Macroscopic differences of the system energy plots can be observed for this test case. Due to the differences recorded in friction forces amplitudes and displacements, this behavior was somewhat expected.

Table 7 compares the ratio Ψ. Regarding computing efficiency for this test case:

– the use of the velocity-based and stick–slip models with a stiff ODE solver is advised;

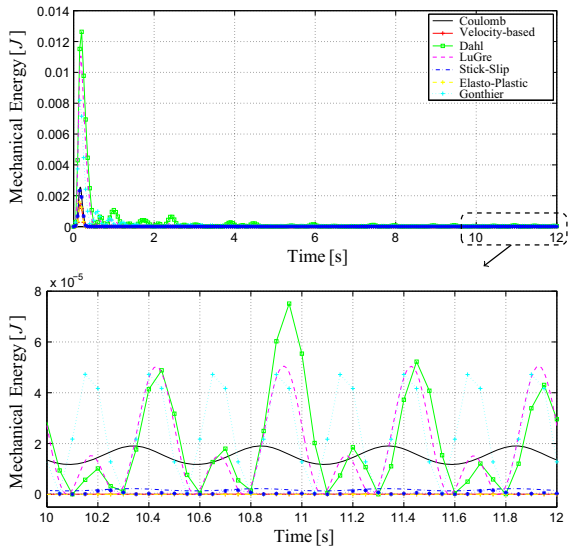

Fig. 25 System kinetic and potential energy for the pre-sliding test case

– the solver `ode15s` is unable to meet the integration tolerance for the Karnopp friction model;
– Coulomb, Dahl, LuGre, elasto-plastic, and Gonthier models are not apparently affected by the choice of the ODE solver and `RelTol` parameter.

4 Conclusions

A review of eight friction models has been presented. The smooth Coulomb, velocity-based, and Karnopp models are based on the Coulomb friction model, whereas the Dahl, LuGre, stick–slip, elasto-plastic, and Gonthier models are established on the bristle approach. The capability of these friction models to mimic physical macroscopic phenomena, such as Stribeck effect, stiction, and pre-sliding displacement, has been herein tested. Some computational issues associated have been also reported.

In particular, three significant test cases have been analyzed in order to compare the performances of the friction models in terms of computational efficiency. Each friction model discussed handles the singularity of the classical Coulomb model at zero relative velocity. Table 8 has been compiled as a summary of the main features of each friction model, such as the number of parameters, the capability of simulating stiction, evaluation of static force, and the presence of pre-sliding displacement.

Table 7 Normalized computing time Ψ [%] for the pre-sliding test case

Model	Solver								
	`ode45`			`ode113`			`ode15s`		
	10^{-4}	10^{-6}	10^{-8}	10^{-4}	10^{-6}	10^{-8}	10^{-4}	10^{-6}	10^{-8}
Coulomb	10	7	7	7	5	5	9	5	5
Velocity based	94	100	95	77	75	76	6	4	4
Dahl	4	4	4	4	5	5	6	6	6
LuGre	4	4	4	5	5	5	7	7	8
Stick–slip	13	15	14	11	11	11	4	4	4
Karnopp	1	1	1	1	1	1	*	*	*
Elasto-plastic	4	4	4	3	3	3	5	5	5
Gonthier	6	10	11	6	10	10	6	10	10

Table 8 Summary of the main features for each friction model

Model	No. parameters	Stiction	Static force	Pre-sliding
Coulomb	2			
Velocity based	4			
Karnopp	3	✓	✓	
Dahl	3	✓		✓
LuGre	7	✓	✓	✓
Stick–slip	4	✓	✓	
Elasto-plastic	8	✓	✓	✓
Gonthier	8	✓	✓	✓

Stick–slip, elasto-plastic, and Gonthier models require the definition of many parameters. On the contrary, the smooth Coulomb, velocity-based, and Karnopp models need a minimum set of parameters and programming skills. The calibration of the model and the identification of the bristle parameters $\sigma_0, \sigma_1, \sigma_2$ require the availability of experimental data.

As it is well known, the smooth Coulomb model is not able to reproduce the stiction phenomenon and the velocity-based model does not produce any force at zero relative velocity. This last model approximates stiction by reducing considerably the relative velocity. The bristle-based models can simulate the pre-sliding effect. However, only the elasto-plastic and the Gonthier models do not introduce any drift.

On the basis of the experience gathered in the numerical tests herein reported:

- the velocity-based model demonstrated to be sensitive to the choice of the ODE solver. A stiff solver, such as the Matlab `ode15s`, considerably improves its computational efficiency;
- the Gonthier and Karnopp models had a low dependency from the ODE solver and `RelTol` value;
- although its implementation for the case of multiple contacts is not straightforward, due to the required evaluation of the external forces acting on each body, the Karnopp model demonstrated excellent computational performances;
- the LuGre and Gonthier models exhibited a good trade-off between the capability of reproducing meaningful friction effects and computational burden for the test cases discussed.

References

1. Al-Bender, F.: Fundamentals of friction modeling. In: ASPE Spring Topical Meeting on Control of Precision Systems (2010)
2. Altpeter, F.: Friction Modeling, Identification and Compensation. Ph.D. thesis, École Polytechnique Fédérale de Lausanne (1999)
3. Andreaus, U., Casini, P.: Dynamics of friction oscillators excited by a moving base and/or driving force. J. Sound Vib. **245**(4), 685–699 (2001)

4. Anitescu, M., Potra, F.: Formulating dynamic multi-rigid-body contact problems with friction as solvable linear complementarity problems. Nonlinear Dyn. **14**(93), 231–247 (1997)
5. Armstrong-Hélouvry, B., Dupont, P., Canudas de Wit, C.: A survey of models, analysis tools and compensation methods for the control of machines with friction. Automatica **30**(7), 1083–1138 (1994)
6. Armstrong-Hélouvry, B., Canudas de Wit, C.: Friction modeling and compensation. In: The Control Handbook. CRC Press, Boca Raton (1995)
7. Åström, K.J., Canudas De Wit, C.: Revisiting the LuGre Model stick–slip motion and rate dependence. IEEE Control Syst. **28**(6), 101–114 (2008)
8. Benson, D.J., Hallquist, J.O.: A single surface contact algorithm for the post-buckling analysis of shell structures. Comput. Method Appl. Mech. Eng. **78**, 141–163 (1990)
9. Berger, E.: Friction modeling for dynamic system simulation. Appl. Mech. Rev. **55**(6), 535 (2002)
10. Bliman, P.A., Sorine, M.: Easy-to-use realistic dry friction models for automatic control. In: 3rd European Control Conference, Rome (Italy), pp. 3788–3794 (1995)
11. Borello, L., Dalla Vedova, M.D.L.: Dry friction discontinuous computational algorithms. Int. J. Eng. Innov. Technol. **3**(8), 1–8 (2014)
12. Bowden, F.P., Leben, L.: The nature of sliding and the analysis of friction. Proc. R. Soc. Lond. Ser. A Math. Phys. Sci. **169**(938), 371–391 (1939)
13. Canudas de Wit, C., Olsson, H., Åström, K.J., Lischinsky, P.: A new model for control of systems with friction. IEEE Trans. Automat. Control **40**(3), 419–425 (1995)
14. Cha, H.Y., Choi, J., Ryu, H.S., Choi, J.H.: Stick–slip algorithm in a tangential contact force model for multi-body system dynamics. J. Mech. Sci. Technol. **25**(7), 1687–1694 (2011)
15. Chou, D.: Dahl Friction Modeling. Ph.D. thesis, Massachusetts Institute of Technology (2004)
16. COMSOL: The Structural Mechanics Module. User's Guide Version 4.3 (2012)
17. Coulomb, P.C.A.: Theorie des machines simples. Bachelier (1821)
18. Dahl, P.R.: Solid friction damping of mechanical vibrations. AIAA J. **14**(12), 1675–1682 (1976)
19. Do, T.N., Tjahjowidodo, T., Lau, M.W.S., Phee, S.J.: Nonlinear modeling and parameter identification of dynamic friction model in tendon sheath for flexible endoscopic systems. In: 10th International Conference on Informatics in Control, Automation and Robotics, pp. 5–10 (2013)
20. Duan, C., Singh, R.: Dynamics of a 3dof torsional system with a dry friction controlled path. J. Sound Vib. **289**, 657–688 (2006)
21. Dupont, P., Armstrong, B., Hayward, V.: Elasto-plastic friction model: contact compliance and stiction. In: Proceedings of the 2000 American Control Conference, vol. 2, pp. 1072–1077 (2000)
22. Dupont, P., Street, C., Hayward, V., Armstrong, B.: Single state elasto-plastic models for friction compensation. IEEE Trans. Automat. Control **47**(5), 787–792 (1999)
23. FunctionBay Inc: RecurDyn Solver Theoretical Manual (2012)
24. Galvanetto, U.: Bifurcations and chaos system with dry friction. J. Sound Vib. **204**(4), 690–695 (1997)
25. Geffen, V.V.: A Study of Friction Models and Friction Compensation. Technische Universiteit Eindhoven, Technical Report (2009)
26. Glocker, C., Pfeiffer, F.: Multiple impacts with friction in rigid multibody systems. Nonlinear Dyn. **7**, 471–497 (1995)
27. Gonthier, Y., McPhee, J., Lange, C., Piedbœuf, J.C.: A regularized contact model with asymmetric damping and dwell-time dependent friction. Multibody Syst. Dyn. **11**(3), 209–233 (2004)
28. Hayward, V., Armstrong, B.: A new computational model of friction applied to haptic rendering. In: Experimental Robotics VI, vol. 250, pp. 403–412. Springer, London (2000)
29. Hinrichs, N., Oestreich, M., Popp, K.: On the modelling of friction oscillators. J. Sound Vib. **216**(3), 435–459 (1998)
30. Karnopp, D.: Computer simulation of stick slip friction in mechanical dynamic systems. J. Dyn. Syst. Meas. Control **107**, 100–103 (1985)
31. Kermani, M., Patel, R., Moallem, M.: Friction identification in robotic manipulators: case studies. In: Proceedings of IEEE Conference on Control Applications, pp. 1170–1175 (2005)
32. Kikuuwe, R., Takesue, N., Sano, A., Mochiyama, H., Fujimoto, H.: Fixed-step friction simulation: from classical coulomb model to modern continuous models. IEEE Int. Conf. Intel. Robot Syst. **1**, 1009–1016 (2005)
33. Kim, T.C., Rook, T.E., Singh, R.: Effect of smoothening functions on the frequency response of an oscillator with clearance non-linearity. J. Sound Vib. **263**(3), 665–678 (2003)
34. Lacoursière, C., Linde, M., Lu, Y., Trinkle, J.: A framework for data exchange and benchmarking of frictional contact solvers in multibody dynamics. In: ECCOMAS Thematic Conference on Multibody Dynamics, pp. 2–3. Barcelona (2015)
35. Liu, H., Song, X., Nanayakkara, T.: Friction estimation based object surface classification for intelligent manipulation. In: IEEE ICRA 2011 Workshop on Autonomous Grasping (2011)
36. LMS International: LMS Virtual. Lab Motion. User's Guide (2012)
37. López, I., Busturia, J., Nijmeijer, H.: Energy dissipation of a friction damper. J. Sound Vib. **278**(3), 539–561 (2004)
38. Marchi, J.A.D.: Modeling of Dynamic Friction , Impact Backlash and Elastic Compliance Nonlinearities in Machine Tools , with Applications To Asymmetric Viscous and Kinetic Friction Identification. Ph.D. thesis, RensselÃęr Polytechnic Institute (1998)
39. Marques, F., Flores, P., Lankarani, H.M.: On the frictional contacts in multibody system dynamics. In: ECCOMAS Thematic Conference on Multibody Dynamics (2015)
40. Márton, L., Kutasi, N.: Practical identification method for striebeck friction. In: Proceedings of the 6th International Symposium of Hungarian Researchers, pp. 425–436 (2005)
41. McMillian, A.J.: A non-linear friction model for self-excited vibrations. J. Sound Vib. **205**(3), 323–335 (1997)
42. Mostaghel, N.: A non-standard analysis approach to systems involving friction. J. Sound Vib. **284**, 583–595 (2005)
43. MSC.Software: Adams/View help (2012)

44. Muvengei, O.: Computational implementation of LuGre friction law in a revolute joint with clearance. In: Proceedings of the 2012 Mechanical Engineering Conference on Sustainable Research and Innovation, vol. 4, pp. 99–108 (2012)
45. Olsson, H., Åström, K.J., Canudas De Wit, C., Gäfvert, M., Lischinsky, P.: Friction models and friction compensation. Eur. J. Control **4**, 176–195 (1998)
46. Pennestrì, E., Toso, M., Rossi, V.: ESA multibody simulator for spacecrafts' ascent and landing in a microgravity environment. CEAS Space J. (2015)
47. Pennestrì, E., Valentini, P.P., Vita, L.: Multibody dynamics simulation of planar linkages with Dahl friction. Multibody Syst. Dyn. **17**, 321–347 (2007)
48. Pfeiffer, F., Glocker, C.: Multibody dynamics with unilateral contact. Wiley-VCH Verlag GmbH & Co., KGaA, Germany (2004)
49. Piatkowski, T.: Dahl and lugre dynamic friction models—the analysis of selected properties. Mech. Mach. Theory **73**, 91–100 (2014)
50. Qi, Z., Xu, Y., Luo, X., Yao, S.: Recursive formulations for multibody systems with frictional joints based on the interaction between bodies. Multibody Syst. Dyn. **24**, 133–166 (2010)
51. Rabinowicz, E.: Stick and slip. Sci. Am. **194**(5), 109–119 (1956)
52. Rao, S.S.: Mechanical Vibrations. Addison-Wesley Longman Incorporated, USA (1986)
53. Richard, C., Cutkosky, M., MacLean, K.: Friction identification for haptic display. Proc. ASME Dyn. Syst. Control Div. **67**, 327–334 (1999)
54. Romano, R.A., Garcia, C.: Karnopp friction model identification for a real control valve. In: Proceedings of the 17th World Congress of The International Federation of Automatic Control, vol. 17, pp. 14906–14911 (2008)
55. Rooney, G., Deravi, P.: Coulomb friction in mechanism sliding joints. Mech. Mach. Theory **17**(3), 207–211 (1982)
56. Simpack: SIMPACK Documentation (2013)
57. Tasora, A.: An iterative fixed-point method for solving large complementarity problems in multibody systems. In: Proceedings of XVI GIMC, Bologna (2006)
58. Thomsen, J.J., Fidlin, A.: Analytical approximations for stick–slip vibration amplitudes. Int. J. Nonlinear Mech. **38**, 389–403 (2003)
59. Threlfall, D.: The inclusion of Coulomb friction in mechanisms programs with particular reference to DRAM. Mech. Mach. Theory **13**(4), 475–483 (1978)
60. Wang, D., Rui, Y.: Simulation of the stick–slip friction between steering shafts using ADAMS. In: International ADAMS User Conference, pp. 1–11 (2000)
61. Wu, S.C., Yang, S.M., Haug, E.J.: Dynamics of mechanical systems with Coulomb friction, stiction, impact and constraint addition–deletion. Mech. Mach. Theory **21**(5), 417–425 (1986)